Energy Conversion and Management 194 (2019) 173–185

Contents lists available at ScienceDirect

Energy Conversion and Management

journal homepage: www.elsevier.com/locate/enconman

Evaluating the benefits of Integrating Floating Photovoltaic and Pumped Storage Power System

Luyao Liu[a], Qie Sun[a,*], Hailong Li[b], Hongyi Yin[a], Xiaohan Ren[a], Ronald Wennersten[a]

[a] Institute of Thermal Science and Technology, Shandong University, Jinan, China
[b] Energy Technology, School of Business, Society and Energy, Mälardalens University, Västerås, Sweden

ARTICLE INFO

Keywords:
Floating photovoltaic
Pumped storage power system
Collaborative operation
Genetic algorithm

ABSTRACT

Floating Photovoltaic systems have developed very fast in recent years. Compared to individual Floating Photovoltaic systems, further advantages, such as grid connectivity and energy storage, can be obtained when Floating Photovoltaic operates collaboratively with Pumped Storage Power Systems. This paper proposed an Integrated Floating Photovoltaic-Pumped Storage Power System and quantitatively assessed the potential of the integrated system in electricity generation and conservation of water and land resource. The study developed a coordinated operation model for the Integrated Floating Photovoltaic-Pumped Storage Power System, which employed a dual-objective optimization, namely to maximize the benefits of electricity generation and to minimize the energy imbalance at the same time. The dual-objective optimization was solved using the genetic algorithm method. Other benefits of the Integrated Floating Photovoltaic-Pumped Storage Power System, namely conservation of water and land resource, were also assessed. The proposed methodology was applied to a 2 GW Floating Photovoltaic farm and a 1 GW Pumped Storage Power System. Results indicated that the Integrated Floating Photovoltaic-Pumped Storage Power System has a great potential for gaining the benefits of electricity generation (9112.74 MWh in a typical sunny day averagely) and reducing energy imbalance (23.06 MW aggregately in one day). The coordinated operation provides the possibility to achieve a higher generation benefits without affecting the reliability of the grid, while the optimization method plays a key role of efficient coordination. In addition, the system would help to save 20.16 km^2 land and 19.06 million m^3 water a year due to the reduction in evaporation loss. The synthetic benefits greatly improve the economic and environmental feasibility of photovoltaic systems in reality.

1. Introduction

According to China's first national water census bulletin (2013) [1], the total number of natural lakes with a surface area of 1 km^2 or larger is 2865 and the total surface area is about 78,000 km^2. However, water resource is unevenly distributed over the country and the volume per capita is very limited. China has constructed 46,758 hydropower stations. However, many of the hydropower stations in recent years could not operate at its full capacity due to insufficient water storage. In addition, the competition for water resource between electricity generation and agricultural production has become increasingly intensive in China [2]. Therefore, it has been crucial and urgent for China to conserve water resource, while promoting sustainable development of renewable energy at the same time [3].

According to China's Intended Nationally Determined Contribution (INDC), China aims to increase the consumption of non-fossil fuels to 20% of the total consumption of primary energy by 2030. By Sep.2018, the total installed capacity of photovoltaic (PV) plants had reached 164.74 GW [4]. Given that traditional terrestrial PV systems require large area of land surface (about 8 m^2 for 1 kW), the development of PV in China is facing enormous challenge about land resource, especially in eastern China.

Based on the above background, Floating PV (FPV) systems, i.e. to install PV cells on a floating system on water surface [5], can offer a synthetic solution for energy production and conservation of water and land resource [6]. Since the first pilot FPV plant was built in California in 2008, over 20 FPV power plants have been built in the world, with the installed capacity from 0.5 kW to 100 MW [7,8]. China is one of the countries with the most developing FPV systems in recent years. Many FPV projects with a total capacity of 1.7 GW has been constructed and this figure will grow to 5GW by the end of 2018 [9].

The advantages of FPV technology has been demonstrated by

* Corresponding author.
E-mail address: qie@sdu.edu.cn (Q. Sun).

https://doi.org/10.1016/j.enconman.2019.04.071
Received 2 January 2019; Received in revised form 8 April 2019; Accepted 24 April 2019
Available online 03 May 2019
0196-8904/

literatures. Choi [10] has claimed that the generation efficiency of FPV systems is 11% higher than conventional terrestrial PV systems due to lower module temperature. Trapani et al. [11] reported that by installing FPV offshore, the limited land resource in the islands of Malta can been largely saved. The literatures [12] and [13] have also elaborated the performance, challenges and environmental impacts of FPV, which support the deployment of FPV.

Moreover, further advantages can be obtained when FPV systems are installed on hydropower reservoirs [14]. An integrated hydro-FPV system cannot only solve the grid-connection problem of regular terrestrial PV systems [15], but also achieve the complementary effects between hydro and solar energy [16]. Kougias et al. [17] proposed to install FPV systems on existing water reservoirs and reported that the combined hydro-FPV system was expected to create mutual gains for both hydropower and solar power. Kougias et al. in [18] described that the close water-energy interrelationship has brought opportunities of achieving the synergy between electricity production and water provision. Beluco and Souza [19] argued that the time complementarity between hydropower and solar energy is beneficial for sizing and operation of integrated hydro-PV systems.

In addition to the aforementioned advantages, a Pumped Storage Power System (PSPS), a special form of hydropower, can complement an FPV power system to achieve energy storage and to address the intermittency problem of solar energy [20]. Kocamana et al. [21] indicated that PSPS can help to improve grid stability, power quality and reliability due to the merits of flexible regulation and strong load-following capability. Ma et al. [22] demonstrated that PSPS have the highest storage capacity and can be more economical than other technologies for energy storage. Patwal et al. [23] investigated the impacts of a PSPS incorporating terrestrial PV power units in India. They found that the integration makes the system more efficient, economically viable, and reliable, which confirmed the advantage of the combination.

Many countries have constructed many PSPS stations over the decades, which ensured a large capacity of complementing renewable energy [24]. Foley et al. [25] performed a technical, economic and environmental long-term generation expansion planning analysis on the integration of PSPS with wind power in the electricity grid system of the Ireland. Dursun et al. [26] also reported adopting pumped storage facilities to accommodate the growing penetration of wind energy and investigated the contribution of wind-hydro pumped storage systems to meeting Turkey's electricity demand. Spain has constructed a PSPS to operate jointly with the wind power plants on the EI Hierro and Canary Islands [27]. Aihara et al. [28] studied the power supply reliability in power system using operation of the PSPS with a large penetration of land PV based on a case study in Japan. Therefore, there should be great potential of solar and hydro energy by the maximum utilization of these renewable sources.

However, there is a lack of study looking into the Integrated Floating PV-Pumped Storage Power System (IFPV-PSPS), and, to the authors' knowledge, there has been few demonstration projects in this form in practice. In principle, an IFPV-PSPS can simultaneously yield multiple benefits: saving terrestrial land, saving water resource and enhancing electricity generation of PV. As regards the methods for the coordination of hydro-PV hybrid systems, An et al. [29] adopted the theories of complimentary hydro-PV operation and detected principles for its short-term scheduling. Ming et al. [30] formulated a robust optimization model to maximize the total energy production in the scheduling of daily generation. Yang et al. [31] developed a long-term multi-objective optimization model for simultaneously maximizing annual power generation and ensuring reliability, and a dynamic programming technique was adopted to solve the optimization problem. In addition, other studies on integrated hydro-PV systems pay their attentions on, e.g., system sizing [32] and control optimization [33], in which the operation scheduling strategy is indispensable. Different from ordinary hydropower plants, a PSPS can generate electricity and restore energy by pumping water. The operation scheduling of a PSPS has recently attracted much attention. Aihara et al. [28] proposed a genetic algorithm and tabu search-based method for scheduling the operation of a PSPS to improve generation benefits and system reliability. In Patwal et al. 's work [31], a crisscross search particle swarm optimization technique was implemented for the scheduling of a PSPS. A common problem in the existing studies is the assumption that the pumping power of a PSPS is adjustable, which, however, is on the contrary. More importantly, a coordinated operation strategy for an IFPV-PSPS has not yet been developed. Furthermore, few studies have systematically considered the associated benefits of an IFPV-PSPS in terms of the preservation of land and water resources.

Therefore, the paper aims to quantitatively assess the potential of the IFPV-PSPS. To this aim, the operation of the IFPV-PSPS was simulated using a Coordinated Operation (CO) model. While there are numerous ways for the two individual systems to operate together, the CO model is optimized to simultaneously maximize the power generation and minimize the energy imbalance using genetic algorithm method. The CO model optimization was implemented under a typical sunny weather condition and the results were further compared with an individual FPV system, an individual PSPS and the plain aggregation of the two individual systems, respectively. In addition, extra benefits of the IFPV-PSPS in terms of water conservation and land saving were assessed.

The remainder of the paper was organized as follows: Section 2 presents the methods of the assessment of IFPV-PSPS, comprising the simulation model used to estimate the energy generation benefits and the method for calculating the water and land saving effect of IFPV-PSPS; Section 3 presents the modelling results of the optimized coordination of the IFPV-PSPS and comparison analysis are made. Finally, Section 4 presents the conclusion of the study.

2. Methods

The method for evaluating the potential of the IFPV-PSPS consists of three steps:

Step 1. The mathematical models for simulating the time series of FPV and PSPS production were established (Section 2.1). Specifically, a Multivariate Non-Linear Regression (MNLR) model for estimating the performance of FPV was built and it was validated using the experimental data from a real FPV station (Section 2.1.1). A model for simulating the performance of the PSPS was constructed, with reference to the working principles of PSPS [34] (Section 2.1.2). The system size and electricity load profile were determined for the study (Section 2.1.3).

Step 2. A CO model for simulating the IFPV-PSPS was developed to estimate the potential of electricity generation (Section 2.2). The CO model employed a dual-objective optimization, namely to maximize the benefits of electricity generation and to minimize the energy imbalance, and the dual-objective optimization was solved by Genetic Algorithm (GA).

Step 3. The approach for assessment of benefits of the IFPV-PSPS in terms of water conservation and land saving was established based on three scenarios. (Section 2.3)

2.1. Mathematical model for Floating Photovoltaic and Pumped Storage Power System

The mathematical models for evaluating the FPV and the PSPS were constructed, and the system size and the electricity load profile are reported in this section.

2.1.1. Mathematical model for evaluating the Floating Photovoltaic

Three types of models can be used to forecast FPV power outputs, and they include: black box methods, e.g. Artificial Neural Network (ANN) based methods [35], decision tree [36] and Support Vector

Machine (SVM) [37], gray box methods, e.g. wavelet neural network [38], and white box methods, e.g. generalized linear model [39]. For the sake of convenience, a Multivariate Non-Linear Regression (MNLR) model [40], which is a statistic white-box model derived based on the physical mechanism of photovoltaic system, was built to forecast the FPV power outputs. It is validated using the experimental data from a 3 kW experimental FPV system in Jinan, China. Enhanced electricity generation can be obtained due to the cooling effect of water body.

Power output can be influenced by various meteorological factors, in which the solar irradiance and temperature are the most significant ones [41]. From the FPV plant, a large amount of irradiance, temperature and power data can be obtained. Data processing technologies provide support for dealing with complex data information and designing statistical model [42]. The MNLR equation with solar irradiance and temperature as variables can be expresses as (1) and (2):

$$P_{PV} = b_0 + b_1 KG + b_2 KGlnG + b_3 KG(lnG)^2 + b_4 KG^2 + b_5 KG^2 lnG + b_6 KG^2 (lnG)^2 \quad (1)$$

$$K = 1 + \varepsilon(T_m - 25°C) \quad (2)$$

where P_{PV} is the PV power output (MW); b_0 is a constant; $b_1 - b_6$ are the regression coefficients; ε is the power-temperature coefficient (/°C), set to be 0.0045; K is the relation weight between power output and temperature; G is the solar irradiance (W/m^2); T_m is the PV module temperature; T_a is the air temperature on the water body. Module temperature T_m can be determined as:

$$T_m = T_a + bG + c \quad (3)$$

where b is the fitting coefficient; c is the constant.

The data on the FPV power output, solar radiation and temperature with an interval of 15 min from January 1 to July 30, 2018 were used to determine the MNLR model. The future power produced P_{PV} by an FPV plant can be expediently forecasted by using the instantaneous meteorological data (forecasted values of solar irradiance G and air temperature T_a). The forecasted solar irradiance and air temperature were obtained from an exogenous source, namely the National Aeronautics and Space Administration (NASA).

When the FPV is integrated with the PSPS, the energy balance of the FPV system at time t can be expressed as:

$$P_{PV,t} = P_{PVL,t} + P_{P,t} + P_{D,t} \quad (4)$$

where P_{PVL} is the electricity delivered to the load; t is time step, which is set as 15 min in this study; P_P is the electricity used for pumping water; P_D is the PV curtailment, referring to the discarded electricity. Other losses are neglected in the study.

2.1.2. Mathematical model for the Pumped Storage Power System

The power output of hydropower at time t can be expressed as Eq. (5).

$$P_{H,t} = \eta_{out} A \rho Q_t \Delta H \quad (5)$$

$$\Delta H = H_{up} - H_{down} \quad (6)$$

where P_H is the electricity output of the hydropower station (W); A is the synthetic output coefficient of the power station, set to be 9.81; η_{out} represents the efficiency of electricity generation, assumed to be 0.75; Q is the discharge flow (m^3/s); ρ is the density of water (1000 kg/m^3) and ΔH is the net water head of the power station (m); H_{up} and H_{down} are the upper and lower water head (m).

The pumped power can be described as Eq. (7).

$$P_{P,t} = \frac{g \rho q_t \Delta h}{\eta_{in}} \quad (7)$$

where η_{in} represents the storage efficiency, assumed to be 0.75; g is gravitational acceleration, 9.8 m^2/s is used in the study; q is the storage inflow (m^3/s), i.e. the volume of water pumped by the electricity from the FPV; Δh is the delivery head (m).

The water balance is defined as:

$$V_{t+1} = V_t + (I_t + q_t - Q_t) \times \Delta t \quad (8)$$

where V is the storage volume in reservoir (m^3); I is the natural runoff (m^3/s). For PSPS, only a small amount of natural runoff is needed for supplementing water evaporation and leakage losses, which is negligible in the operation; t + 1 is the next time step; Δt is the length of the time step (s). Considering the storage and outflows of the reservoir associated with the PSPS, the water balance can be further expressed as:

$$V_{t+1} = V_t + \left(I_t + \frac{\eta_{in} P_{P,t}}{g \times \Delta h_t} - \frac{P_{H,t}}{\eta_{out} \times A \times \Delta H_t} \right) \times \Delta t \quad (9)$$

The storage capacity *Vcap* is also required, which should be no less than the difference between the maximum and minimum values $V_t^{max} - V_t^{min}$ simulated over the period. In addition, a nonlinear function f(x) was adopted to express the relationship between the storage V and water level L according to the reservoir characteristic:

$$V_t = f(L_t) \cup L_t = f^{-1}(V_t) \quad (10)$$

2.1.3. System size and electricity load

The collaborative performance of an IFPV-PSPS is affected by the relative size of the FPV and the PSPS [43]. While optimization of the size of the FPV and the PSPS is out of the paper's scope, the paper referred to a real PSPS, i.e. the Taian PSH station with a capacity of 1GW, as the study project and assumed the capacity of the integrated FPV P_{PVcap} to be 2 GW, according to the proposed size in [44]. The PSPS consists of four reversible pump turbines/generator motors with a capacity (P_{Pcap}, P_{Hcap}) of 250 MW each. The Taian PSPS operates to stabilize the electricity output of the FPV and meet the electricity loads at the same time. The electricity output of the 2GW FPV system is calculated according to the experimental FPV system in Jinan [45]. The details of the PSPS can be seen in Table 1.

The rated power of the load P_{LI} was set as 1000 MW and the daily dynamic load was determined according to a typical daily electricity load in the geographical area under study (Fig. 1) [46]. The time interval of the data is 15 min.

As shown in Fig. 1, the daily load contains two peaks, namely one in the morning and the other in the evening. When the load cannot be fully met by the amount of electricity from the IFPV-PSPS, it will resort to the grid.

The actual load P_L that can be met by the IFPV-PSPS is determined according to an iterative process as shown by Eq. (11) and follows the energy balance restrictions (12)–(14).

$$P_{L,t} = P_{LI,t} \times \frac{\sum_{t=1}^{T} P_{PV,t} - \sum_{t=1}^{T} P_{P,t} - \sum_{t=1}^{T} P_{D,t} + \sum_{t=1}^{T} P_{H,t}}{\sum_{t=1}^{T} P_{LI,t}} = P_{LI,t} \times \frac{E_{PV} - E_P - E_D + E_H}{E_{LI}} \quad (11)$$

Table 1
Parameters of PSPS in the designed IFPV-PSPS system.

Parameter	Value
Total hydropower capacity	1 GW
Pumped capacity	1 GW
Individual hydropower capacity	250 MW
Units number	4
Coefficient	0.75
Upper reservoir storage volume	11.076 million m^3
Generation storage volume	8.9511 million m^3
Lower reservoir storage volume	29.93 million m^3
Upper reservoir area	1.432 km^2
Lower reservoir area	84.53 km^2
Relative water head	248 m

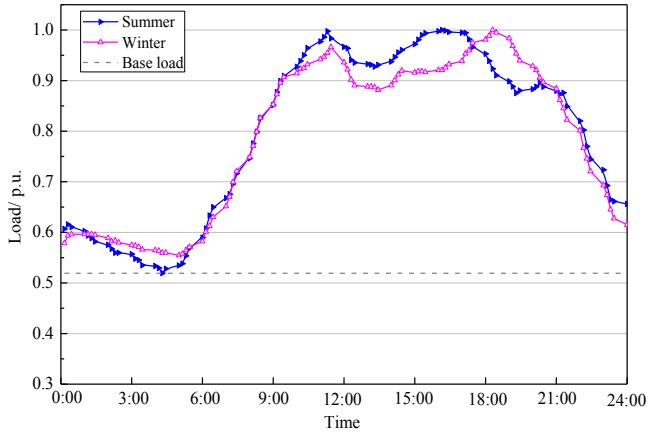

Fig. 1. The load variation on a typical day in Shandong power grid in summer and winter.

s. t.

$$E_{PV} = E_{PVL} + E_P + E_D \tag{12}$$

$$E_{PV} - E_P - E_D + E_H = E_{CO} \tag{13}$$

$$E_{CO} + E_R = E_L \tag{14}$$

where E_{PV} is the generation energy of PV during the regulation period (MWh); E_P is the total pump energy during the day (MWh); E_{PVL} is the total PV power generation to the load during the day (MWh); E_D is the total discarded energy during the day (MWh); E_H is the total amount of hydropower generation power energy during the day (MWh); E_{CO} is the total amount of power generation by the integrated system during the day (MWh); E_R is the total amount of reserve power (MWh), with the initial value being 0; E_{LI} is the total amount of electricity load with initial value being 1000 MW (MWh); E_L is the total amount of actual electricity load (MWh).

2.2. Coordinated operation model for the integrated Floating Photovoltaic-Pumped Storage Power System

A CO model was developed to optimize the operation of the IFPV-PSPS. The CO model employed a dual-objective optimization, namely to maximize the benefits of electricity generation and meanwhile to minimize the energy imbalance, and the dual-objective optimization was solved by GA.

2.2.1. The coordinated operation model with dual-objective

As the electricity output from the IFPV-PSPS is not always consistent with the dynamic load, the imbalance between them is defined as Regulation Power Source (RPS), $\Delta P_{R,t}$, determined as Eqs. (15) and (16):

$$P_{L,t} = P_{PVL,t} + P_{H,t} + \Delta P_{R,t} \tag{15}$$

$$\Delta P_{R,t} = \begin{Bmatrix} P_{R1,t},\ P_{R1,t} < 0 if P_{PVL,t} + P_{H,t} > P_{L,t} \\ P_{R2,t},\ P_{R2,t} > 0 if P_{PVL,t} + P_{H,t} < P_{L,t} \end{Bmatrix} \tag{16}$$

where P_L is the dynamic electricity load; P_{PVL} is the excessive electricity from the FPV; P_H is the power output of the hydropower plant; ΔP_R is the RPS, i.e. the imbalance between the output of the IFPV-PSPS and the dynamic load; P_{R1} is the excessive electricity of the IFPV-PSPS over the dynamic load; P_{R2} is the amount of electricity deficit when the IFPV-PSPS cannot meet the dynamic load.

The CO model employed a dual-objective optimization and the first objective is to obtain the maximum generation benefits of the IFPV-PSPS on the premise of maximizing the utilization of solar energy (see Eq. (17)).

Table 2
The range of the parameters $P_{H,t}$ and $P_{P,t}$.

Unit type	Generation	Pumping
Conventional units	$0 \sim P_N$	0, P_N
Variable-speed units	$0 \sim P_N$	$0.5P_N \sim P_N$

$$F_1 = max \sum_{t=1}^{T} (P_{PVL,t} + P_{H,t}) \tag{17}$$

where the time periods T is 96 in an operational day pursuant to the time interval of 15 mins. The sum of $P_{PVL,t}$ and $P_{H,t}$ is actually the coordinated power output $P_{CO,t}$ of the integrated system.

The second objective is to minimize the imbalance between the electricity output of the IFPV-PSPS and the electricity load, which is expressed as:

$$F_2 = min \sqrt{\frac{1}{T} \sum_{t=1}^{T} \Delta P_{R,t}{}^2} \tag{18}$$

In the optimization process, the PSPS adjusts its operation by scheduling $P_{H,t}$ and $P_{P,t}$, while the FPV regulate its operation by dispatching $P_{PVL,t}$, to simultaneously achieve the maximum power generation and minimum the energy imbalance. The range of the parameters are shown in Table 2, where P_N is the rated pump/ generation capacity of the unit.

2.2.2. The collaborative strategy and genetic algorithm method to solve the dual-objective optimization

Since existing operating strategies of FPV and PSPS systems are developed independently [47], a collaborative strategy was employed to optimize the collaborative operation of the IFPV-PSPS, i.e. the electricity generated by the FPV system is used for water pumping in the first place and the excessive electricity from the FPV is then used to meet the electricity load. The dispatch of PV electricity output is illustrated in Fig. 2.

Based upon the collaborative operation strategy, the dual-objective optimization problem was solved using the GA method, with the advantages of simplicity, easy implementation and having a lot of successful practice applications. The first step was to determine the initial values of the CO power in the GA optimization, as indicated in Fig. 2, and it helps to improve the computation efficiency. If the excessive PV power, $P_{PVE,t}$, is larger than the load, $P_{L,t}$, the CO power, $P_{CO,t}$, increases from the load value $P_{L,t}$ with an increase coefficient R, which is a random number between 1 and 1.3. In this process, the CO power, $P_{CO,t}$, can be adjusted to gain more benefits from power generation. If the excessive PV power, $P_{PVE,t}$, is smaller than the load, $P_{L,t}$, the CO power $P_{CO,t}$ is equal to the load, $P_{L,t}$. The initial values of the CO power, $P_{CO,t}$ (t = 1, 2⋯,96), were acquired using pre-optimization before the GA optimization.

With the initial values of the CO power, the dual-objective optimization problem was then solved using the GA method. The GA method operates on a population of chromosomes, which are initialized, evaluated, selected, crossed-over and mutated along the generations to find the best solutions to the CO of the IFPV-PSPS [48]. The results from the GA optimization is a set of pairwise values for the two objectives, often called the Pareto Frontier [49]. The process of the GA optimization is illustrated at the bottom of Fig. 2. The detailed parameter settings adopted in the GA method can be found in Appendix A.

2.2.3. Constraints to the coordinated operation model

The constraints *to the CO model* and the associated dual-objective optimization are as follows.

$$P_{P,t}^{min} \le P_{P,t} \le P_{P,t}^{max} \tag{19}$$

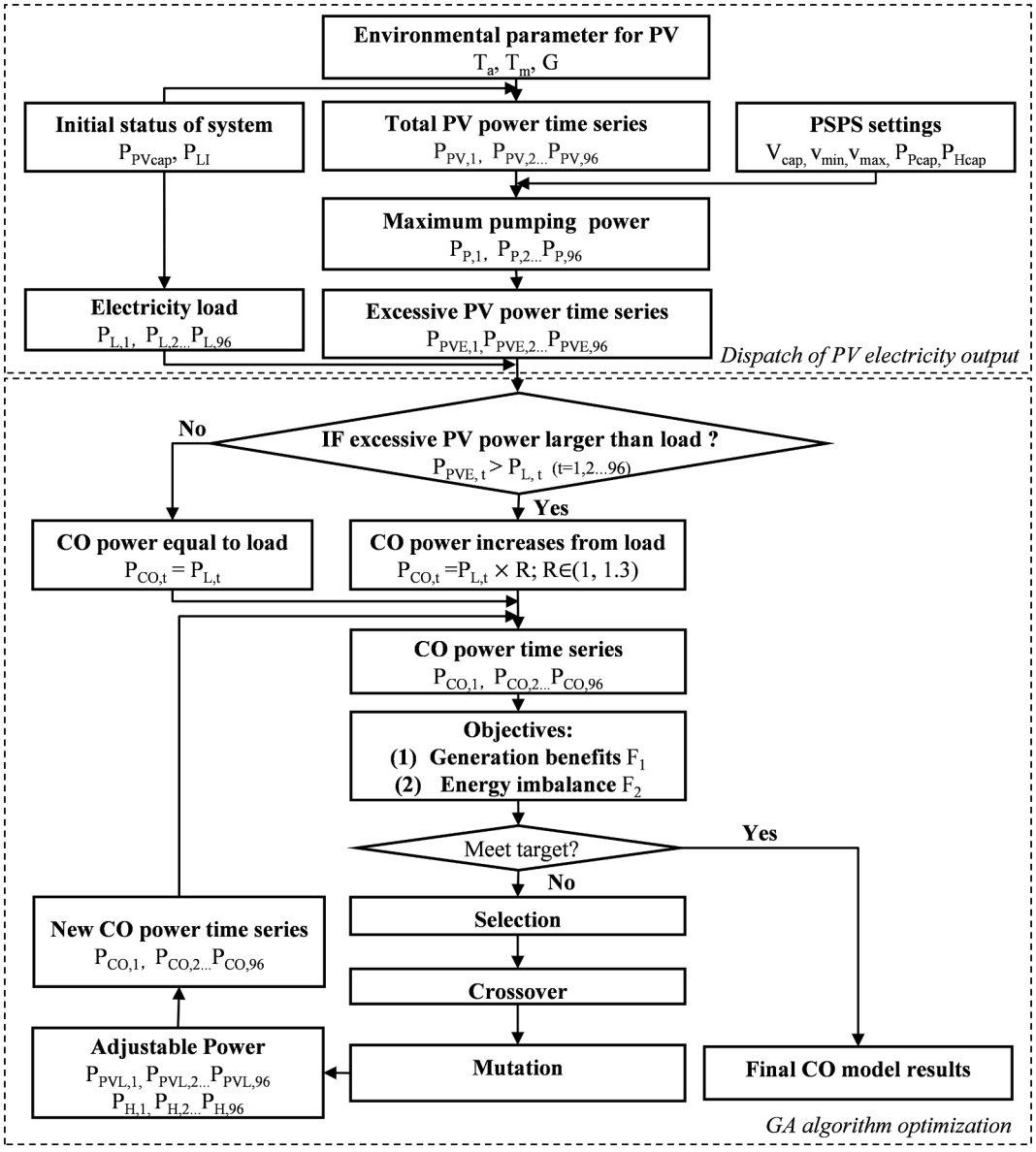

Fig. 2. The collaborative operation strategy and the GA method to solve the dual-objective optimization.

$$P_{H,t}^{min} \le P_{H,t} \le P_{H,t}^{max} \quad (20)$$

$$0 \le P_{PVL,t} \le P_{PV,t} - P_{P,t} \quad (21)$$

$$(1-\varepsilon)P_{L,t} \le P_{H,t} + P_{PVL,t} \le (1+\varepsilon)P_{L,t} \quad (22)$$

$$N_{H,t}^{min} \le N_{H,t} \le N_{H,t}^{max} \quad (23)$$

$$N_{P,t}^{min} \le N_{P,t} \le N_{P,t}^{max} \quad (24)$$

$$N_t^{min} \le N_{H,t} + N_{P,t} \le N_t^{max} \quad (25)$$

$$V_t^{min} \le V_t \le V_t^{max} \quad (26)$$

$$V_t^{max} - V_t^{min} \le V_{cap} \quad (27)$$

$$v^{min} \le V_{96} - V_1 \le v^{max} \quad (28)$$

$$H_t^{min} \le H_t \le H_t^{max} \quad (29)$$

$$L_t^{min} \le L_t \le L_t^{max} \quad (30)$$

where $P_{P,t}^{min}$ and $P_{P,t}^{max}$ are the lower and upper limit of pumping power at time period *t*; $P_{H,t}^{min}$ and $P_{H,t}^{max}$ are the lower and upper limit of electricity output by the hydropower plant at time *t*, set as 0 and 250 MW; Eq. (22) restricts the deviation degree of coordinated output to load, whileε indicates the deviation coefficient towards load, set as 0.3 in this study; $N_{H,t}$ and $N_{P,t}$ are the number of units for generation and pumping in operation; $N_{H,t}^{min}$ and $N_{H,t}^{max}$ are the minimum and maximum number of generation units to start up, which are 0 and 4; $N_{P,t}^{min}$ and $N_{P,t}^{max}$ are the minimum and maximum number of pumping units to start up; N_t^{min} and N_t^{max} are the minimum and maximum number of units, which are 0 and 4 in this study; V_t denotes the real-time water volume at time t; V_t^{min} and V_t^{max} are the lower and upper limit of water storage at time *t*; The difference between the maximum and minimum values of water volume $V_t^{max} - V_t^{min}$ over the period, is required to be no more than the storage capacity V_{cap} for the IFPV-PSPS; The $V_{96} - V_1$ is the water volume change of the day, with the V_{96} and V_1 as the water volume at the end and at the beginning of the day; v^{min} and v^{max} are the acceptable change in the volume of water storage, set as -250 and 250 thousand m^3; $H_t^{min}$and $H_t^{max}$are the lower and upper limit of water head at time *t;* L_t^{min} and $L_t^{max}$are the lower and upper limit of water level at time *t*, respectively.

Table 3
Power density of existing FPV installations.

Plant Name	Size	Power Capacity	Power Density
Kato-Shi [50]	31300 m^2	2.87 MW_P	91.69 MW_P/km^2
Otae & Jipyeong Reservoir [51]	52600 m^2	6 MW_P	113.95 MW_P/km^2
Umenoki	74300 m^2	7.75 MW_P	104.31 MW_P/km^2
QE II Reservoir	57500 m^2	6.33 MW_P	110.09 MW_P/km^2
Yamakura Reservoir [52]	180000 m^2	13.7 MW_p	76.11 MW_P/km^2
Overall	301100 m^2	31.05 MW_P	99.23 MW_P/km^2

Source: [53].

2.3. Benefits of saving in land and water resource

The methods for evaluating the potential of the FPV in land conservation and water saving are reported in this section.

2.3.1. Land saving effect

The study evaluates the effect of the FPV on land saving via the parameter power density (MWp/km^2), which measures the installed capacity of an FPV system on a unit area of water surface. Table 3 compiles the power density of existing FPV installations in the world, which have an average power density of 99.23 MWp/ km^2.

Based on the average power density, the technical capacity and generation potential of the water bodies (reservoir, lake, canal, etc.) for installing FPV systems was further evaluated.

$$\text{Technical capacity potential} = urban\ openspace \times power\ density \tag{31}$$

$$\text{Technical generation potential} = \sum \begin{bmatrix} urban\ openspace \times power\ density \\ \times\ capacity\ factor \times operating\ hours \end{bmatrix} \tag{32}$$

2.3.2. Water saving effect

With growing demand for water, the water saving effect is an important benefit of the system [54]. In general, an FPV system covers a large area of water surface and thus is able to save water resource by reducing water evaporation loss, which is the direct water-saving effect of the FPV system. When an FPV system is installed on the reservoir of a PSPS, the electricity generated by the PV system can be used to substitute the electricity generated by the hydropower station, via supplying electricity to end users or pumping water, and this is equivalent to saving the water consumption of the PSPS. This is called indirect water-saving effect in the paper.

Regarding the direct water-saving effect, there is a variety of methodologies for estimating the water loss due to evaporation and the Penman-Monteith method is the most widely used one [55], which is complex and out of the scope of this study. Therefore, the study used an ordinary method and assumed that: 1) the evaporation is proportional to the exposed surface area of the water body and 2) the evaporation rate is uniform across the entire surface of the water body. Therefore, the direct water-saving effect can be calculated as Eq. (33) according to [56]:

$$E = E_0 \times C \times p \tag{33}$$

where E means the amount of avoided evaporation due to the installation of the FPV system and E_0 represents the amount of evaporation losses under natural conditions, which is 0.9–1.2 million m^3 (MCM) per km^2 for the project under study [57]; C is the area of covered water surface; p is the prevention coefficient, assumed to be 0.9 in the study.

The indirect-water saving effect is calculated by converting the amount of electricity generation by the FPV system into the volume of water consumed by the hydropower station, as shown by Eq. (34).

$$V_e = \frac{0.75 \times 3600 \times E_{PV,e} \times (1 - \epsilon)}{\rho \times g \times \Delta H} \tag{34}$$

where V_e is the volume of water resource (m^3); $E_{PV,e}$ is power generation of the FPV system (Wh); ϵ is the discarding rate of PV power, which is ratio of discarded PV output E_D to the total amount of electricity generated by the FPV system E_{PV}; ΔH is the water head of the PSPS (m).

3. Results

The results of the generation potential based on CO optimization of the IFPV-PSPS and the benefits of water and land conservation are presented in this section.

3.1. Modelling results of the Floating Photovoltaic, integrated Floating Photovoltaic-Pumped Storage Power System and Pumped Storage Power System

The results in terms of power generation of the FPV, optimal CO of the IFPV-PSPS and operation of the PSPS are reported in this section.

3.1.1. Power generation of the Floating Photovoltaic

The FPV power output on a typical sunny day was evaluated to examine the above proposed methodology. The most notable distinction of FPV output in cloudy and rainy days from that in a sunny day is the reduction in the output. Since this study concentrates on the optimization of the CO of the IFPV-PSPS, the variations in the output, as well as related uncertainty in the output forecast, go beyond the scope of the study. In addition, the output in a sunny day can be regarded as a nominal value for estimating the potential of the IFPV-PSPS.

Ambient temperature is an important parameter that can affect the working performance of PV systems. In general, the FPV module has a lower working temperature than an equivalent terrestrial module due to the cooling effect of the water body. This effect can be clearly seen in the measured data from the experimental FPV system in Jinan (Fig. 3).

Based on the empirical model from Cheng C's work [58], the relationship between module temperature T_m of monocrystalline silicon FPV cells and air temperature on water surface T_a can be determined as:

$$T_m = T_a + 0.0145G - 2.8148 \tag{35}$$

For comparison, the equation between land PV module temperature T_{ml} and air temperature T_{al} on land is:

$$T_{ml} = T_{al} + 0.0130G - 0.5898 \tag{36}$$

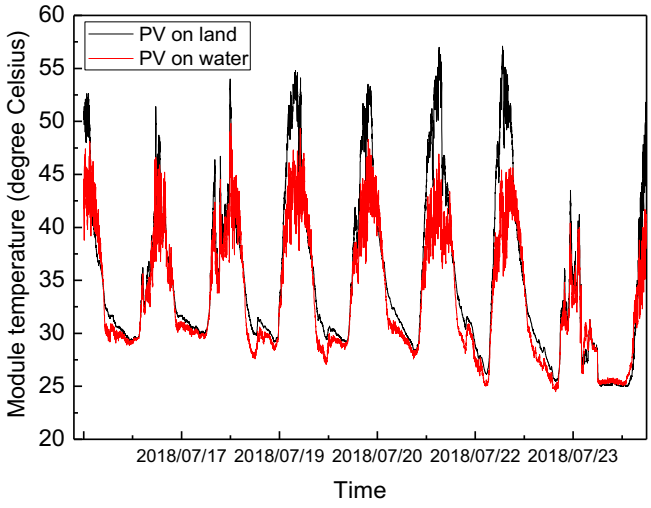

Fig. 3. Module temperature of an FPV system and a terrestrial PV system under a sunny weather.

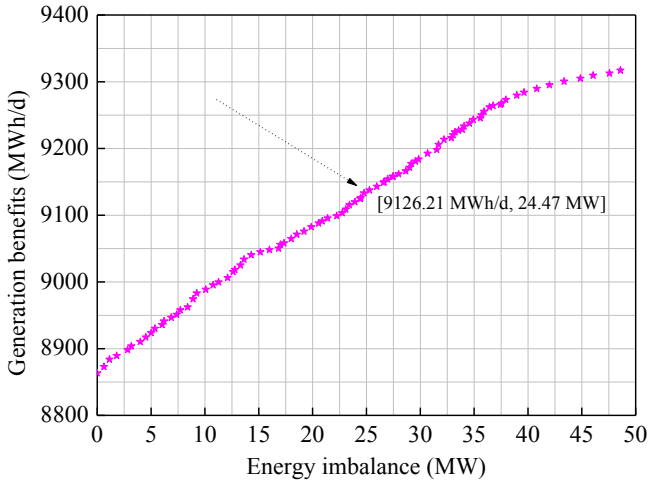

Fig. 4. Pareto Front of the proposed multi-objective CO model for the IFPV-PSPS.

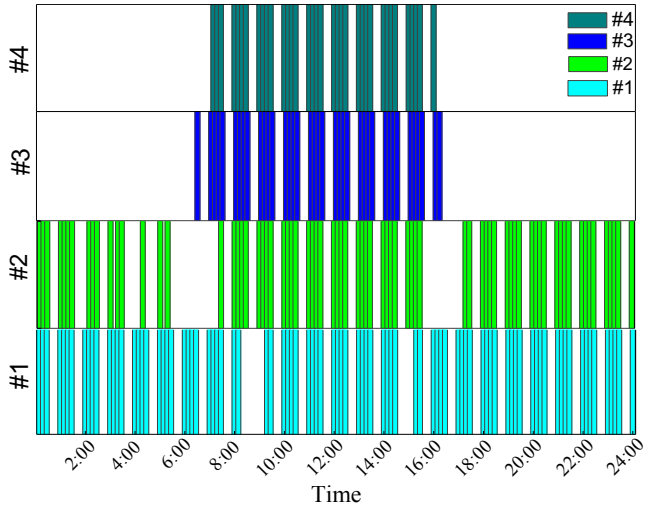

Fig. 5. Operation schedule of PSPS in CO process for the optimal solution.

where G is the solar irradiance (W/m^2).

By comparing Eqs. (35) and (36), the PV module temperature on water surface can achieve lower value than PV module on land, with an average temperature difference of about 4 °C, which will lead to a difference of 1.8% in power generation efficiency.

Validated by the measured data from the experimental FPV system in Jinan, the power output of the FPV systems under sunny weather conditions can be expressed as in Eq. (37):

$$P_{PV,t} = 7.520KG(t) - 8.87KGlnG(t) + 3.967KGln^2G(t) - 2.300KG^2(t) + 0.542KG^2lnG(t) - 0.024KG^2ln^2G(t) + 47.67(\text{MW}) \quad (37)$$

Therefore, the electricity output from the FPV was forecasted with a fifteen-minute interval, which is taken as the boundary condition for the dual-objective CO model.

3.1.2. Optimal coordinated operation of the integrated Floating Photovoltaic-Pumped Storage Power System

The non-inferior solutions to the CO model, known as the Pareto Front, were obtained by solving the dual-objective optimization problem (Fig. 4 and Table 4). The results represent the average values of 1000 iterations of a one-day solution.

As indicated by Fig. 4, a larger generation benefit corresponds to a larger imbalance between the electricity output and the load. The statistical characteristics of the results are shown in Table 4. On average, the proposed IFPV-PSPS system is able to produce 9112.74 MWh generation benefits in one day and the energy imbalance can be restricted to 23.06 MW.

Since the optimal results of the IFPV-PSPS include many CO schemes regarding the dual-objectives of electricity generation and energy imbalance, a CO schemes with the status of [9126.21 MWh/d, 24.47 MW] in Fig. 4 is randomly selected for demonstration. The following analysis can also be applied to other status.

3.1.3. Operation of the Pumped Storage Power System

The operation scheduling of the PSPS under the demonstrated CO scheme can be seen in Fig. 5. The four reversible pump turbines/generator motors have a capacity of 250 MW each. A column in Fig. 5 at a time point represents that the turbine/generator is in operation and otherwise it is in the idle state. Correspondingly, the accumulated volume of pumped water by the IFPV-PSPS and water storage in the reservoir are shown in Fig. 6.

The power generation by PSPS is 4701.37 MWh/d, about half of the total electricity output of the IFPV-PSPS. Due to the supplement by the pumped water using surplus energy from IFPV-PSPS, the daily water consumption of the IFPV-PSPS is restricted to a very low level, i.e. 25.85 * 10^4 m^3/day or 28.33 m^3/MWh, and this is owing to the collaborative operation strategy, i.e. the electricity generated by the FPV is stored by pumping water.

In addition to the scheduling of PSPS, the specific data of the dispatching of FPV power underlying the selected CO scheme of in support of the comparison analysis in Section 3.2 is also listed additionally in Appendix C.

3.2. Comparison between the integrated Floating Photovoltaic-Pumped Storage Power System and stand-alone systems

The performance of the IFPV-PSPS is compared with a stand-alone FPV, a stand-alone PSPS and the plain aggregation of an FPV and a PSPS without optimal CO to reveal the potential of the proposed system.

3.2.1. Comparison between the Integrated Floating Photovoltaic-Pumped Storage Power System and a stand-alone Floating Photovoltaic system

The power output of the IFPV-PSPS in this status is shown in Fig. 7. For comparison, the power output from a hypothetical stand-alone FPV system of the same capacity was simulated to compare with the IFPV-PSPS as that in Fig. B.1 in Appendix B. The results on the benefits of electricity generation and on the energy imbalance were computed and reported in Table 5. The specific data in support of Table 5 could be found in Appendix C.

The following results have been derived (Fig. 7 and Table 5).

- With the CO model, the output of the IFPV-PSPS can well follow the

Table 4
Characteristics of the dual objectives on a regular day.

	Energy generation benefits (MWh/day)				Energy imbalance (MW)			
	min	Max	average	Std.	min	max	average	Std.
The day	8863.38	9317.18	9112.74	127.86	0	48.59	23.06	12.74

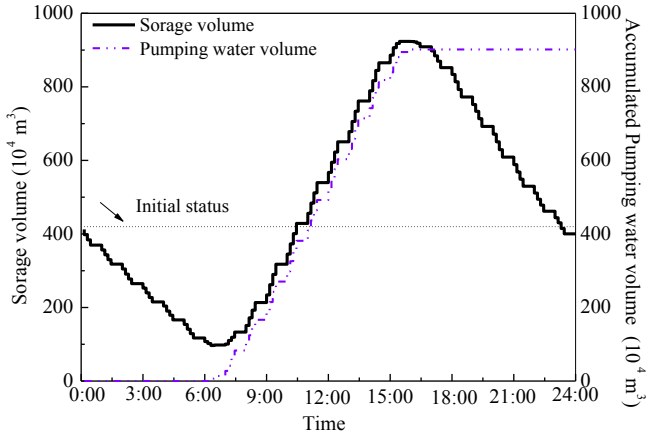

Fig. 6. The accumulated volume of pumped water by the IFPV-PSPS and water storage in the reservoir.

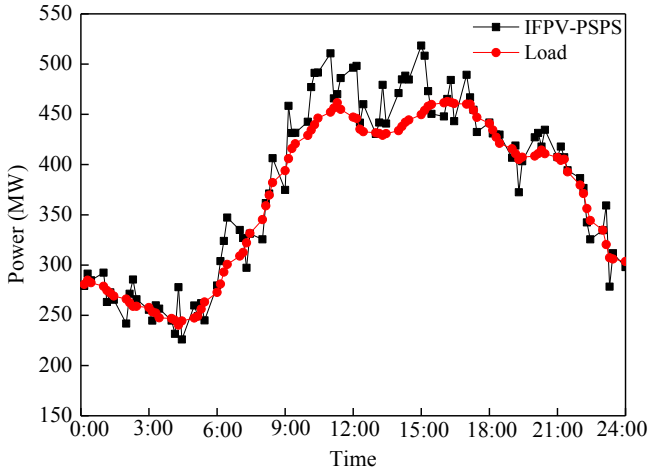

Fig. 7. The power output of the IFPV-PSPS and matching with load in one day.

load curve. Therefore, the energy imbalance between the output of the IFPV-PSPS and the load is much smaller than the imbalance between a stand-alone FPV and the load. This implies a significant improvement in the system stability and reliability.

- The overall utilization rate of the electricity from the FPV increase from 31.82% in the stand-alone FPV system to 86.62% in the IFPV-PSPS. While the electricity from the FPV directly to the load remains nearly the same, 56.08% of the total amount of electricity is used for pumping water, which can be further used to generate electricity. In the meantime, the curtailment of the FPV outputs is reduced from 68.18% to 13.38%.
- As a result, the IFPV-PSPS can produce a total of 9126.21 MWh electricity benefits in one day, much more than 4610.68 MWh/d from a stand-alone FPV system.

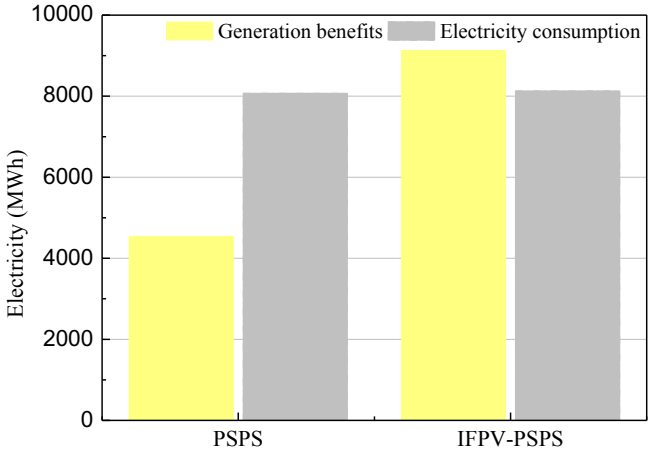

Fig. 8. Comparison between an IFPV-PSPS and a stand-alone PSPS.

3.2.2. Comparison between the integrated Floating Photovoltaic-Pumped Storage Power System and a stand-alone Pumped Storage Power System

The IFPV-PSPS is further compared with a stand-alone PSPS in this section.

For a regular stand-alone PSPS, water is pumped to the upper reservoir using the electricity from the grid during the load valley, while water is discharged to the lower reservoir for power generation at the load peak. Therefore, the generation benefits of a stand-alone PSPS and the amount of electricity consumption for water pumping can be calculated as Eqs. (38) and (39).

$$\begin{cases} E_{H,S} = \frac{3600 \times V_{cap}}{0.75 \times \rho \times g \times \Delta H} (Generation\ \ mode) & (38) \\ E_{P,S} = \frac{0.75 \times 3600 \times V_{cap}}{\rho \times g \times \Delta H} (Pumping\ \ mode) & (39) \end{cases}$$

where $E_{H,S}$ refers to the generation benefits of the PSPS; and $E_{P,S}$ is the electricity consumption of the PSPS from the power grid.

For a stand-alone PSPS of the same capacity as that in the IFPV-PSPS, the generation benefit is 4701.37 MWh/d, much less than 9126.21 MW/d from the IFPV-PSPS (Fig. 8). In the meantime, the electricity consumption of the stand-alone PSPS is 8065.54 MWh, which requires a large amount of costs and leads to additional environmental emissions.

Based upon comparison analysis, the superiorities of IFPV-PSPS than stand-alone systems were validated. In truth, the superiorities rely on the combination of the two kinds of systems. i.e. the FPV and PSPS interact with each other and achieves complementarity. The PSPS improves the utilization rate of PV power and address the intermittency problem of PV, while FPV could provide electricity for pumping water that reduces the costs of PSPS, the which a win–win cooperation.

3.2.3. Comparison between the integrated Floating Photovoltaic-Pumped Storage Power System and the plain aggregation of a Floating Photovoltaic and a Pumped Storage Power System

There are numerous ways for the FPV and the PSPS work together.

Table 5
Comparison of the IFPV-PSPS and a stand-alone FPV system.

	Generation Benefits (MWh/day)	Energy imbalance (MW)	FPV power to load (MWh)	FPV power for pumping water (MWh)	FPV power curtailment (MWh)	Total Power (MWh)
IFPV-PSPS	9126.21	24.47	4424.84 (30.54%)	8125.00 (56.08%)	1938.45 (13.38%)	14488.29 (100%)
Stand-alone FPV	4610.68	744.27	4610.68 (31.82%)	0 (0%)	9877.61 (68.18%)	14488.29 (100%)

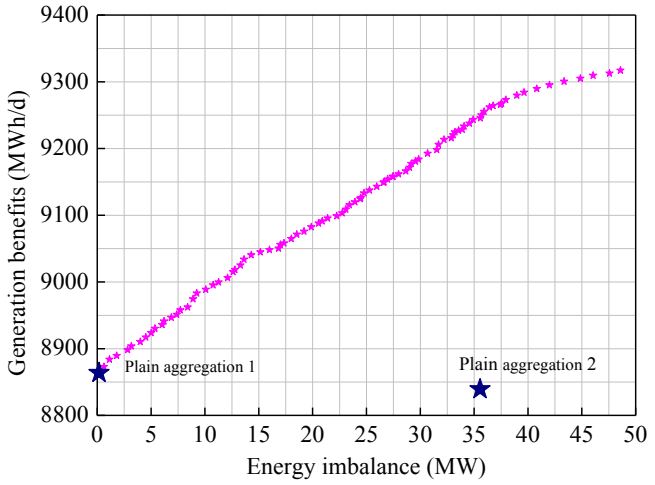

Fig. 9. Generation benefits and energy imbalance of the plain aggregation of two individual systems and comparison with the Pareto Frontier.

In order to indicate the advantages of the proposed FPV-PSPS system under the optimal CO, the generation benefits and related energy imbalance of the plain aggregation of two individual systems were calculated and compared with the Pareto Frontier, as shown in Fig. 9, with the blue stars representing the results of the plain aggregation. The differences can be regarded as the results of optimization.

The CO scheme under zero energy imbalance [8863.38 MWh/d, 0 MW] can be regarded as the best result for the plain aggregation of the two stand-alone. The effects of energy imbalance from 0 MW to 50 MW on generation benefits through adjusting power scheduling and dispatching are investigated through the Pareto Frontier optimal solution set, illustrating that generation benefits increase remarkably as energy imbalance rises. The coordinated generation benefits are augmented by 1.4% and 2.5% respectively when 10 MW and 20 MW energy imbalance. The generation benefits can be further enhanced by about 5.1% (generation benefits: 9317.18MWh/d) if an energy balance of 50 MW is allowed.

The CO scheme [8838.86 MWh/d, 36.10 MW] is another solution of the plain aggregation of the two stand-alone systems. It is obvious the performance in terms of generation benefits and associated energy imbalance without coordination management is inferior than that under CO model optimization.

3.3. Benefits on savings in land and water resource

The associated benefits of IFPV-PSPS in light of land and water saving is also discussed to provide references for decision making. The land saving effect and water conservation benefits are reported in Table 6.

(a) Saving in land

- With the energy density of 99.23 MW/km^2, the required water surface area for installing the 2 GW FPV system is 20.16 km^2. This corresponds to a saving of 20.16 km^2 land resource, if the same capacity of PV system were to be installed on land. The coverage rate of the water surface is 23.85% for the Taian PSPS's reservoir (84.53 km^2) and this will create very minor impacts on the reservoir and related activities, e.g. tourism and fish farming.
- Based on the same principle of the FPV system, the potential for savings in land resource in Shandong is over 210 km^2 with the technical capacity of 20.84 GW, given a mild coverage rate of the water surface of 10%. To make a comparison, the installed PV capacity in Shandong is 10.52 GW at the end of 2017 and is aiming to achieve 18 GW in 2022 and 24 GW capacity till 2028 [59]. Therefore, the large technical potential capacity of FPV will definitely accelerate the development of PV industry in Shandong. In addition, the corresponding technical generation potential of FPV is anticipated to be 11.05 TWh/y, with FPV utilization rate of 20% and working period of 2920 h/year.
- The potential of Shandong Province can be extended to other areas in China, especially the provinces in eastern China, where terrestrial land resource is very limited, especially for large scale deployment of PV systems. There is a total of around 125 thousand km^2 water surface in China and the technical potential capacity for FPV systems can reach 180 GW, with a very conservative coverage rate of only 1.5%. To make a comparison, the amount of China's PV installed capacity is 164.74 GW, of which the distributed PV capacity is 46.80 GW by Sep. 2018 [60]. Therefore, the FPV will boost the development of PV industry in China as an innovative and prospective power generation technology.

(b) Saving in water resource

- The direct water-saving effect is calculated as the avoided evaporation loss and the proposed IFPV-PSPS system can preserve water resource 16.33–21.78 MCM every year, and this amount is about twice the generation capacity of the reservoir.
- The indirect water-saving effect is calculated as the savings in water consumption of the hydropower station. Based on the IFPV-PSPS system, the annual electricity generation from FPV systems could reach about 1.06 TWh/y, with the FPV utilization rate of 20%. Take the average PV power discarding rate ϵ to be 13%, the PV power will correspond to further indirect water savings of about 1020 MCM.
- Since there is great uncertainty, the calculation results of nationwide land and water saving of FPV is undetermined and open for discussion.

4. Conclusion

The fluctuations and uncertainties in PV outputs have created great challenges to practical utilization of solar energy. This paper presents a novel form of multi-energy system, namely an IFPV-PSPS to achieve

Table 6
Summary of land saving and water saving effect of FPV in the paper and potential area.

	Water area (km^2)	Occupying rate	FPV occupying area (km^2)	Technical capacity potential (GW)	Technical generation potential (TWh/y)	Direct water saving (MCM/y)	Indirect water saving (MCM/y)
FPV in the paper	84.53	23.85%	20.16	2	1.06	19.06	1020.00
FPV in Shandong	2100.00	10%	210	20.84	11.05	198.61	10628.40
FPV in China	124700.00	1.5%	1870.5	185.57	/	/	/

synergetic benefits by CO of the PSPS and the FPV system. The paper developed a dual-objective optimization model for the CO of the IFPV-PSPS, which simultaneously maximizes the generation benefits and minimizes the energy imbalance between the generation and the load. The CO optimization model was solved using the GA method on the prerequisite of a collaborative strategy.

The main findings include: the IFPV-PSPS, which includes a 2 GW FPV and a 1 GW PSPS, can gain considerable generation benefits, i.e. on average 9112.74 MWh a day, and minimize energy imbalance between the IFPV-PSPS and the load to 23.06 MW. The superiority of the proposed IFPV-PSPS was further supported by comparing the IFPV-PSPS with a stand-alone FPV and a stand-alone PSPS, while the effectiveness of the proposed model was verified by calculating the generation benefits and related energy imbalance of the plain aggregation of two stand-alone systems and comparing with the Pareto Frontier. With additional benefits in saving terrestrial land, the IFPV-PSPS enables another practical option for the deployment of PV, especially where land resource is limited. The IFPV-PSPS can also been seen as an efficient means to alleviate the water scarcity with an enormous water saving potential, both directly by avoiding evaporation and indirectly by pumping water.

In addition, the study makes contributions to the academic area with the following implications:

- The proposed collaborative strategy can help to make a pre-optimization and decrease the number of decision variables to be optimized. This enables the GA method to solve more complex dual-objective problems.
- The dual-objective optimization model is a generic approach that can be easily applied to other CO of integrated energy systems. Notably, the present study indicates that CO provides the possibility to achieve a higher utilization rate of intermittent renewable energy without affecting the reliability of the grid, while the optimization method plays a key role of efficient utilization.
- System sizing is another important issue for IFPV-PSPS. The load at night is only satisfied by the PSPS, while the electricity output from the FPV at daytime does not only suffice for the load, but also pumps up water to save energy and also to maintain water balance. Therefore, the capacity of the FPV is usually larger than the capacity of the PSPS.
- The accuracy of PV power forecasts has influence on the coordinated optimization of the integrated system. Thus, quantification of the uncertainty using, e.g. probability interval method based on deterministic point forecasts, will help to improve the optimization process. For a further interest in the quantification of uncertainties, as well as the probability distribution of forecast errors, please refer to, e.g. Liu et al. [41].
- On a higher political level, the development of FPV technology can greatly contribute to China's INDC, as well as to the long-term energy transition.

Declaration of interests

None.

Acknowledgements

This work was supported by Project U1864202 supported by National Natural Science Foundation of China and the Fundamental Research Funds of Shandong University 2018JC060.

Appendix A

The detailed parameter settings in the solving process using GA method are listed in Table A.1.

Table A.1
The summarized parameter settings for GA optimization.

Model parameter	Value	Annotation
Input 1	$P_{L,t}(t = 1, 2\cdots,96)$	Section 2.2.2
Input 2	$P_{PV,t}(t = 1, 2\cdots,96)$	Section 2.1.1
Input 3	$P_{P,t}(t = 1, 2\cdots,96)$	Section 2.2.2
Decision variables	$P_{H,t}$, $P_{PVL,t}(t = 1, 2\cdots,96)$	Section 2.2.2
Number of variables	192	Section 2.2.2
Constraints	Eqs. (19)–(30)	Section 2.2.3
The first objective function F_1	$F_1 = max\sum_{t=1}^{96}(P_{PVL,t} + P_{H,t})$	Eq. (17) in Section 2.2.1
The second objective function F_2	$F_2 = min\sqrt{\frac{1}{T}\sum_{t=1}^{T}\Delta P_{R,t}{}^2}$	Eq. (18) in Section 2.2.1
Weight coefficient transform	$u = F_1 + 100000/F_2$	u is the evaluation function in dual-objective problems
Number of population size	200	/
Number of iterations	1000	/
Evolution rate	0.2	
Coding method	Gray code	

Appendix B

Fig. B.1.

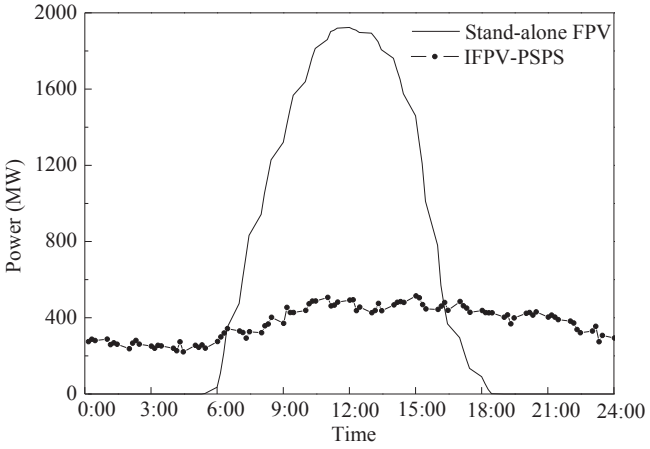

Fig. B.1. The comparison of power output from the stand-alone FPV and IFPV-PSPS.

Appendix C

Table C.1.

Table C.1
Scheduling of PSPS and dispatching of FPV electricity power.

Time	P_{PV}/MW	P_{PVL}/MW	P_P/MW	P_D/MW	P_H/MW	P_{CO}/MW	Load/MW	ΔP_R/MW
0:15	0	0	0	0	279.32	279.32	280.74	1.42
0:30	0	0	0	0	291.45	291.45	284.88	−6.57
0:45	0	0	0	0	284.84	284.84	282.46	−2.38
1:00	0	0	0	0	292.47	292.47	278.85	−13.62
1:15	0	0	0	0	263.19	263.19	274.64	11.44
1:30	0	0	0	0	272.81	272.81	272.21	−0.60
1:45	0	0	0	0	265.53	265.53	269.20	3.67
2:00	0	0	0	0	241.80	241.80	266.18	24.38
2:15	0	0	0	0	271.41	271.41	262.58	−8.83
2:30	0	0	0	0	285.57	285.57	258.97	−26.60
2:45	0	0	0	0	265.97	265.97	258.93	−7.04
3:00	0	0	0	0	255.47	255.47	257.71	2.24
3:15	0	0	0	0	244.71	244.71	253.49	8.79
3:30	0	0	0	0	259.84	259.84	252.27	−7.57
3:45	0	0	0	0	256.59	256.59	247.46	−9.12
4:00	0	0	0	0	244.69	244.69	246.83	2.14
4:15	0	0	0	0	231.50	231.50	245.00	13.50
4:30	0	0	0	0	277.94	277.94	240.19	−37.75
4:45	0	0	0	0	225.95	225.95	244.33	18.38
5:00	0	0	0	0	259.70	259.70	247.29	−12.41
5:15	0	0	0	0	249.11	249.11	249.04	−0.07
5:30	0	0	0	0	262.01	262.01	256.15	−5.86
5:45	2.67	2.67	0	0	242.30	244.96	263.27	18.30
6:00	35.87	35.87	0	0	243.77	279.63	272.78	−6.85
6:15	108.89	108.89	0	0	194.96	303.85	281.10	−22.75
6:30	213.47	213.47	0	0	110.53	324.00	292.98	−31.02
6:45	347.29	97.29	250.00	0	249.96	347.25	300.68	−46.57
7:00	474.49	224.49	250.00	0	110.35	334.84	309.00	−25.84
7:15	598.84	98.84	500.00	0	228.06	326.90	312.55	−14.36
7:30	714.09	214.09	500.00	0	83.17	297.26	322.04	24.78
7:45	832.04	82.04	750.00	0	249.19	331.23	331.54	0.31
8:00	942.27	192.27	750.00	0	133.29	325.55	345.22	19.66
8:15	1052.89	302.89	750.00	0	58.75	361.64	358.89	−2.75
8:30	1138.67	371.20	750.00	17.47	0	371.20	369.59	−1.61
8:45	1228.89	406.34	750.00	72.55	0	406.34	382.08	−24.26
9:00	1320.44	374.75	750.00	195.69	0	374.75	393.96	19.21
9:15	1407.11	458.48	750.00	198.63	0	458.48	405.84	−52.63
9:30	1490.22	431.40	1000.00	58.83	0	431.40	415.95	−15.44
9:45	1567.56	431.58	1000.00	135.98	0	431.58	420.68	−10.89
10:00	1638.67	442.62	1000.00	196.05	0	442.62	429.00	−13.62

(*continued on next page*)

Table C.1 (*continued*)

Time	P_{PV}/MW	P_{PVL}/MW	P_P/MW	P_D/MW	P_H/MW	P_{CO}/MW	Load/MW	ΔP_R/MW
10:15	1699.11	477.08	1000.00	222.03	0	477.08	434.32	−42.76
10:30	1763.11	491.24	1000.00	271.87	0	491.24	439.66	−51.58
10:45	1813.33	491.58	1000.00	321.76	0	491.58	446.18	−45.40
11:00	1859.56	510.71	1000.00	348.85	0	510.71	452.11	−58.60
11:15	1901.78	465.84	1000.00	435.94	0	465.84	456.23	−9.61
11:30	1908.44	470.07	1000.00	438.37	0	470.07	461.57	−8.50
11:45	1919.56	486.06	1000.00	433.49	0	486.06	454.99	−31.08
12:00	1923.56	496.41	1000.00	427.14	0	496.41	447.18	−49.23
12:15	1915.11	498.17	1000.00	416.94	0	498.17	445.96	−52.20
12:30	1909.33	441.69	1000.00	467.64	0	441.69	435.20	−6.49
12:45	1897.33	460.07	1000.00	437.27	0	460.07	432.78	−27.29
13:00	1893.33	430.46	1000.00	462.87	0	430.46	431.56	1.10
13:15	1872.00	441.78	1000.00	430.22	0	441.78	430.93	−10.85
13:30	1848.89	479.33	1000.00	369.56	0	479.33	429.10	−50.23
13:45	1806.67	440.85	1000.00	365.82	0	440.85	430.85	−10.00
14:00	1761.78	471.13	1000.00	290.65	0	471.13	433.78	−37.35
14:15	1704.00	484.68	1000.00	219.32	0	484.68	437.92	−46.76
14:30	1651.11	488.43	1000.00	162.68	0	488.43	442.06	−46.37
14:45	1575.56	484.58	1000.00	90.97	0	484.58	444.42	−40.16
15:00	1459.56	518.46	750.00	191.10	0	518.46	449.75	−68.71
15:15	1332.44	508.35	750.00	74.10	0	508.35	453.88	−54.46
15:30	1208.89	458.89	750.00	0	14.20	473.09	458.02	−15.06
15:45	1011.11	261.11	750.00	0	189.36	450.47	459.77	9.31
16:00	780.27	280.27	500.00	0	167.64	447.91	461.53	13.62
16:15	570.62	320.62	250.00	0	144.66	465.29	462.69	−2.60
16:30	460.44	460.44	0	0	23.70	484.15	462.06	−22.09
16:45	367.82	367.82	0	0	75.39	443.21	460.82	17.61
17:00	295.64	295.64	0	0	193.70	489.35	460.19	−29.16
17:15	238.98	238.98	0	0	227.86	466.84	460.15	−6.69
17:30	184.27	184.27	0	0	270.24	454.51	454.16	−0.35
17:45	134.67	134.67	0	0	297.67	432.34	446.97	14.63
18:00	91.02	91.02	0	0	350.81	441.83	440.98	−0.86
18:15	54.89	54.89	0	0	376.05	430.94	434.38	3.43
18:30	22.84	22.84	0	0	407.09	429.94	427.18	−2.75
18:45	1.78	1.78	0	0	428.06	429.84	421.19	−8.64
19:00	0	0	0	0	406.76	406.76	415.79	9.04
19:15	0	0	0	0	418.94	418.94	410.99	−7.96
19:30	0	0	0	0	372.43	372.43	405.00	32.56
19:45	0	0	0	0	403.29	403.29	407.34	4.05
20:00	0	0	0	0	427.09	427.09	408.50	−18.58
20:15	0	0	0	0	431.49	431.49	410.85	−20.64
20:30	0	0	0	0	417.85	417.85	414.38	−3.48
20:45	0	0	0	0	434.68	434.68	410.77	−23.91
21:00	0	0	0	0	407.49	407.49	407.16	−0.33
21:15	0	0	0	0	417.88	417.88	404.15	−13.73
21:30	0	0	0	0	407.20	407.20	405.31	−1.89
21:45	0	0	0	0	394.29	394.29	392.76	−1.53
22:00	0	0	0	0	386.41	386.41	379.60	−6.81
22:15	0	0	0	0	376.69	376.69	371.22	−5.47
22:30	0	0	0	0	342.47	342.47	356.27	13.80
22:45	0	0	0	0	325.60	325.60	344.31	18.71
23:00	0	0	0	0	334.63	334.63	334.75	0.12
23:15	0	0	0	0	359.29	359.29	320.41	−38.88
23:30	0	0	0	0	278.53	278.53	307.25	28.71
23:45	0	0	0	0	311.80	311.80	306.02	−5.78
24:00	0	0	0	0	297.99	297.99	303.60	5.61

Statistic of power generation/MWh

E_{PV}	14488.29
E_{PVL}	4424.84
E_P	8125.00
E_D	1938.45
E_H	4701.37
E_{CO}	9126.21
E_L	8863.38
E_R	262.83

References

[1] The Ministry of water resources of the People's Republic of China and the statistics of the people's Republic of China 2013. National water resources survey of the first time. China water conservancy, 2013,1-3.
[2] Zeng X, Huang G, Li Y, et al. A multi-reservoir based water-hydro energy management model for identifying the risk horizon of regional resources-energy policy under uncertainties. Energy Convers Manage 2017;143:66–84.
[3] Wang Z, Sun Q, Wennersten R. Outline of principles for building scenarios – transition toward more sustainable energy systems. Appl Energy 2017;185:1890–8.
[4] Su S, Yuan G. International clean energy development report. Social Science Literature Press; 2016.
[5] Liu L, Wang Q, Lin H, et al. Power generation efficiency and prospects of floating photovoltaic systems ☆. Energy Procedia 2017;105:1136–42.
[6] Campanaa P, Wästhagea L, Nookueaa W, Tan Y, Yan J. Optimization and assessment of floating and floating-tracking PV systems integrated in on- and off-grid hybrid energy systems. Solar Energy 2019;177:782–95.
[7] Trapani Kim, Santafé Miguel Redón. A review of floating photovoltaic installations:2007–2013. Prog Photovoltaics: Res Appl 2015;23:524–32.
[8] Chen D. New opportunities, development and challenges for China's aquatic photovoltaic power stations. Electron Prod World 2017;24(5):3–5.
[9] Planning Report on Water Surface Photovoltaic Power Generation in Coal Mining Subsidence Area of Huaihe River and Huaihe River (2016-2018).
[10] Choi Y. A study on power generation analysis of floating PV system considering environmental impact. Int J Software Eng Appl 2014;8(1):75–84.
[11] Trapani K, Millar DL. Proposing offshore photovoltaic (PV) technology to the energy mix of the Maltese islands. Energy Convers Manage 2013;67:18–26.
[12] Trapani K, Redón Santafé M. A review of floating photovoltaic installations: 2007–2013. Prog Photovoltaics Res Appl 2015;23(4):524–32.
[13] Sahu A, Yadav N, Sudhakar K. Floating photovoltaic power plant: a review. Renew Sustain Energy Rev 2016;66:815–24.
[14] Silvério N, Barros R, Filho G, et al. Use of floating PV plants for coordinated operation with hydropower plants: case study of the hydroelectric plants of the São Francisco River basin. Energy Convers Manage 2018;171:339–49.
[15] Liu L, Liu D, Sun Q, et al. Forecasting power output of photovoltaic system using a BP network method. Energy Procedia 2017;142:780–6.
[16] Liu L, Sun Q, Wang Y, Ronald W, Liu Y. Research on short-term optimization for integrated hydro-PV power system based on genetic algorithm. Energy Procedia 2018;152:1097–102.
[17] Kougias I, Bódis K, Jäger-Waldau A, et al. The potential of water infrastructure to accommodate solar PV systems in Mediterranean islands. Sol Energy 2016;136:174–82.
[18] Kougias I, Szabó S, Monforti-Ferrario F, et al. A methodology for optimization of the complementarity between small-hydropower plants and solar PV systems. Renew Energy 2016;87(2):1023–30.
[19] Beluco A, Souza PKD, Krenzinger A. A method to evaluate the effect of complementarity in time between hydro and solar energy on the performance of hybrid hydro PV generating plants. Renew Energy 2012;45(3):24–30.
[20] Aihara R, Yokoyama A, Nomiyama F, et al. Optimal operation scheduling of pumped storage hydro power plant in power system with a large penetration of photovoltaic generation using genetic algorithm. PowerTech, IEEE Trondheim. IEEE; 2011. p. 1–8.
[21] Kocaman AS, Modi V. Value of pumped hydro storage in a hybrid energy generation and allocation system. Appl Energy 2017;205:1202–15.
[22] Ma T, Yang H, Lu L. Feasibility study and economic analysis of pumped hydro-storage and battery storage for a renewable energy powered island. Energy Convers Manage 2014;79:387–97.
[23] Patwal RS, Narang N. Crisscross PSO algorithm for multi-objective generation scheduling of pumped storage hydrothermal system incorporating solar units[J]. Energy Convers Manage 2018;169:238–54.
[24] http://www.sohu.com/a/213122341_99962115.
[25] Foley AM, Leahy PG, Li K, et al. A long-term analysis of pumped hydro storage to firm wind power. Appl Energy 2015;137:638–48.
[26] Dursun B, Alboyaci B. The contribution of wind-hydro pumped storage systems in meeting Turkey's electric energy demand. Renew Sustain Energy Rev 2010;14(7):1979–88.
[27] Pérez-Díaz JI, Perea A, Wilhelmi JR. Optimal short-term operation and sizing of pumped-storage power plants in systems with high penetration of wind energy. Energy Market. IEEE; 2010. p. 1–6.
[28] Aihara R, Yokoyama A, Nomiyama F, et al. Optimal operation scheduling of pumped storage hydro power plant in power system with a large penetration of photovoltaic generation using genetic algorithm. Powertech, IEEE Trondheim. IEEE; 2011.
[29] An Y, Fang W, Ming B, et al. Theories and methodology of complementary hydro/photovoltaic operation: applications to short-term scheduling. J Renew Sustain Energy 2015;7(6):063133.
[30] Bo M, Pan L, Lei C, et al. Optimal daily generation scheduling of large hydro–photovoltaic hybrid power plants. Energy Convers Manage 2018;171:528–40.
[31] Yang Z, Liu P, Cheng L, et al. Deriving operating rules for a large-scale hydro-photovoltaic power system using implicit stochastic optimization. J Cleaner Prod 2018. S095965261831494X.
[32] Mahmoudimehr J, Shabani M. Optimal design of hybrid photovoltaic-hydroelectric standalone energy system for north and south of Iran. Renew Energy 2018;115:238–51.
[33] Huang D, Shen H, Yang XY, et al. Research on a new control strategy of multi-energy complementary isolated power system. Adv Mater Res 2012;614–615:1027–32.
[34] Ming B, Liu P, Chang J, et al. Deriving operating rules of pumped water storage using multi-objective optimization: case study of the Han to Wei Inter-Basin Water Transfer Project, China. J Water Resour Plann Manage 2017(10):143.
[35] Wang Y, Lin H, Liu Y, Sun Q, Wennersten R. Management of household electricity consumption under price-based demand response scheme. J Cleaner Prod 2018;204:926–38.
[36] Lin H, Liu Y, Sun Q, et al. The impact of electric vehicle penetration and charging patterns on the management of energy hub – a multi-agent system simulation. Appl Energy 2018;230:189–206.
[37] Liu L, Zhao Y, Sun Q, et al. Prediction of short-term output of photovoltaic system based on generalized regression neural network. Conference on Energy Internet and Energy System Integration. IEEE; 2017. p. 1–6.
[38] Paulescu M, Brabec M, Boata R, et al. Structured, physically inspired (gray box) models versus black box modeling for forecasting the output power of photovoltaic plants. Energy 2017;121:792–802.
[39] Li Y, He Y, Su Y, et al. Forecasting the daily power output of a grid-connected photovoltaic system based on multivariate adaptive regression splines. Appl Energy 2016;180:392–401.
[40] Zhong J, Liu L, Sun Q. Prediction of photovoltaic power generation based on general regression and back propagation neural network. Energy Procedia 2018;152:1224–9.
[41] Liu L, Zhao Y, Chang D, Xie J, Ma Z, Sun Q, et al. Prediction of short-term PV power output and uncertainty analysis. Appl Energy 2018;228:700–11.
[42] Ma Z, Xie J, Li H, Sun Q, Si Z, Zhang J, et al. The role of data analysis in the development of intelligent energy networks. IEEE Network 2017;31(5):88–95.
[43] Erdinc O, Uzunoglu M. Optimum design of hybrid renewable energy systems: overview of different approaches. Renew Sustain Energy Rev 2012;16:1412–25.
[44] Yufu Wang. Chile Tarapaca pumped storage-photovoltaic solar combined power station project. Water Conserv Hydropower Express 2017;38(1):18–9.
[45] Liu Y. Research on wind and solar hybrid generation technology based on pumped storage. Nanchang University; 2015.
[46] Zhao L, Sha Z, Dong S. Necessity of pumped storage power station construction in Shandong Power Grid. Power and Energy 2012;33(3):266–70.
[47] Lin H, Wang Q, Wang Y, Liu Y, Sun Q, Wennersten R. The energy-saving potential of an office under different pricing mechanisms – application of an agent-based model. Appl Energy 2017;202:248–58.
[48] Ismail MS, Moghavvemi M, Mahlia TMI. Genetic algorithm based optimization on modeling and design of hybrid renewable energy systems. Energy Convers Manage 2014;85(9):120–30.
[49] Chen Y, Li H, He B, et al. Multi-objective genetic algorithm based innovative wind farm layout optimization method. Energy Convers Manage 2015;105:1318–27.
[50] Kyocera TCL Solar Inaugurates Floating Mega Solar Power Plants in Hyogo Prefecture, Japan; 1.7MW and 1.2MW installations will provide equivalent power for roughly 920 average households. News Releases. KYOCERA. https://global.kyocera.com/news/2015/0401_tome.html.
[51] A total of 6 MW photovoltaic hydropower stations have been built in Korea. The power generation capacity is monitored by wireless monitoring at http://www.china-epc.org/zixun/2015-12-21/10265.html.
[52] KYOCERA TCL Solar Begins Construction on 13.7MW Floating Solar Power Plant; Company's fourth floating solar project, world's largest, will be built on Japan's Yamakura Dam reservoir|News Releases|KYOCERA https://global.kyocera.com/news/2016/0102_knds.html.
[53] HARTZELL, TYNAN SCOTT. Evaluating potential for floating solar installations on Arizona water management infrastructure. 2016.
[54] Roger K, Liebi M, Heimdal J, et al. Controlling water evaporation through self-assembly [Applied Physical Sciences]. Proc Natl Acad Sci USA 2016;113(37):10275.
[55] Monteith JL. Evaporation and the environment. In: Fogg GE, editor. The state and movement of water in living organisms. London: Cambridge University Press; 1965.
[56] Zhang Y, Shi K. Study on evaporation-preventing effect of using evaporation-control hollow plastic board to cover the surface of plain reservoirs. Water Saving Irrigation 2014;5:11–3.
[57] Implementation Plan of Comprehensive Regulation of Groundwater Overexploitation Area in Shandong Province. Bulletin of Shandong Provincial People's Government, 2015 (33).
[58] Cheng X, Tan Z. A temperature prediction method for PV modules. Internet Things Technol 2013;11:32–3.
[59] New Energy Industry Development Plan of Shandong Province (2018-2028). People's Government of Shandong Province. 2018.09.17.
[60] From January to September 2018, China's new installed capacity of photovoltaic power generation was 34,544,000 kW distributed photovoltaic, up 12% year-on-year Jibang New Energy Network https://www.energytrend.cn/news/20181120-51484.html.